GEOPHYSICS, VOL. 74, NO. 2 (MARCH-APRIL 2009); P. O17–O28, 16 FIGS., 4 TABLES.
10.1190/1.3054659

Estimation of thickness and velocity changes of injected carbon dioxide layers from prestack time-lapse seismic data

Amir Ghaderi[1] and Martin Landrø[1]

ABSTRACT

In this study, we bring together the two main categories of time-lapse seismic analysis — amplitude analysis and time-shift analysis — to estimate simultaneously the changes in thickness and velocity of a 4D seismic anomaly. The methodology is applied to time-lapse seismic monitoring of carbon dioxide (CO_2) storage at Sleipner field, Norway, that shows significant 4D effects. The 4D anomalies resulting from CO_2 injection appear as a multilayer reflection pattern within the relatively shallow Utsira Sand. This multireflective appearance within the sand layer is interpreted as CO_2 layers trapped below thin shale layers. Because most of the CO_2 layers are believed to be thin (0–20 m), the interference between top and base of these layers needs to be taken into account in 4D seismic analysis. By studying the reflected event from a horizon below the Utsira Sand, we estimate 4D traveltime shifts caused by the presence of the CO_2 layer above this horizon. We then combine these traveltime shifts with measured amplitude changes for the top and base of the CO_2 layer to estimate velocity and thickness changes for the thin CO_2 layer. In 1999, after three years of injection, the most likely velocity change was around 200 m/s and the thickness of the CO_2 layer was around 15 m. In 2001, the corresponding velocity change and thickness estimates were 400 m/s and 15 m, respectively. Finally, in 2002, the most likely velocity change was 500 m/s and the thickness of the CO_2 layer was 15 m. It is not straightforward to apply this method to a stack of CO_2 layers because 4D time shifts below the Utsira Sand only provide information about the average time shift for all layers. The amplitude information for each individual CO_2 layer cannot be resolved without knowing the velocity change within each layer. However, our result from a single CO_2 layer may be used to constrain the velocity changes for the multilayer CO_2 case.

INTRODUCTION

Time-lapse seismic analysis can be divided into two main categories: amplitude analysis and time-shift analysis. These complementary methods often can be used to increase the knowledge of intrareservoir changes (Landrø et al., 2001). For compacting reservoirs, time shift has been the major technique (Guilbot and Smith, 2002; Landrø and Stammeijer, 2004; Hatchell and Bourne, 2005) for qualitative and quantitative 4D analysis. When the same velocities are used for the base and monitor surveys, offset-dependent correction terms are necessary for mid- and far-offset stacks, as discussed by Landrø and Janssen (2002) and Landrø and Stammeijer (2004).

If an accurate velocity analysis is performed separately for the base and monitor surveys (which might be necessary if the time-lapse velocity changes are significant), then this correction term is unnecessary. However, as shown by Kvam and Landrø (2005), it is often difficult to do accurate time-lapse velocity analysis, and then one must take into account the uncertainty in the velocity analysis. Hence, in the presence of the correction term, the poststack traveltime shift cannot be translated directly into velocity changes. Landrø and Stammeijer (2004), assuming zero compaction, and Ghaderi and Landrø (2005) show for prestack seismic data that

$$\frac{\Delta t}{t} \approx -\frac{\Delta V}{V}, \tag{1}$$

where t is the seismic two-way time thickness of the layer and v is the velocity of the layer. In equation 1 it is assumed that $\Delta V \ll V$ and that the change in the incidence angle θ caused by CO_2 injection is negligible. Also note that equation 1 is valid for all offsets, but the assumption that $\Delta\theta$ is small is, of course, less valid for higher offsets.

Manuscript received by the Editor 30 November 2007; revised manuscript received 16 May 2008; published online 12 February 2009.
[1]Norwegian University of Science and Technology, Department of Petroleum Engineering and Applied Geophysics, Trondheim, Norway. E-mail: ghaderi@ntnu.no; mlan@ipt.ntnu.no.

So far we have assumed that the velocity anomaly is constant within the offset span used for the analysis. In the Sleipner CO_2 data set, the typical lateral extension of the CO_2 anomaly is of the order of 750–1500 m. The maximum offset available for the prestack data is 1668 m. This means that edge effects will play an important role for the long-offset time-shift analysis. Hence, a correction formula is needed that can be applied to long-offset data. For this purpose, it is possible to modify the result by Røste et al. (2006). However, in our data example from the Sleipner CO_2 project, we use small-offset prestack seismic data, corresponding to a single offset of 318 m. Thus, the correction formula by Røste et al. (2006) is assumed to have negligible effect.

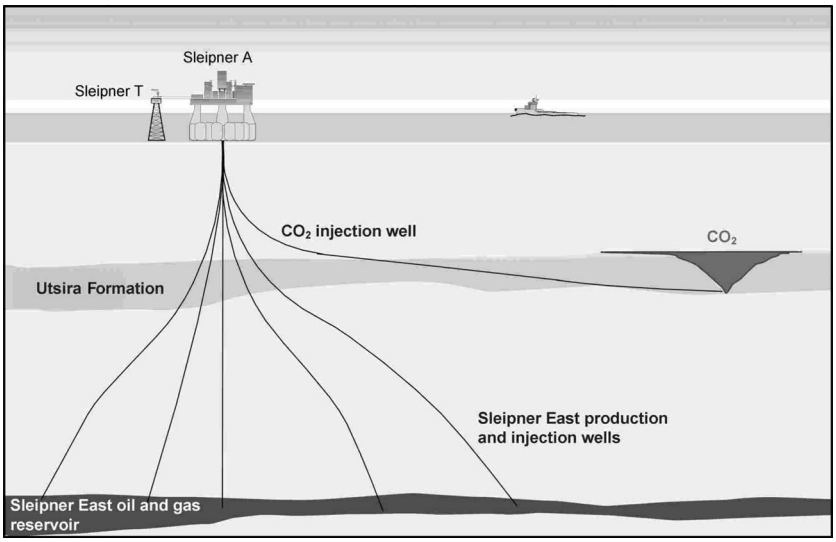

Figure 1. Schematic of CO_2 injection in the Utsira Formation at Sleipner (courtesy of Statoil).

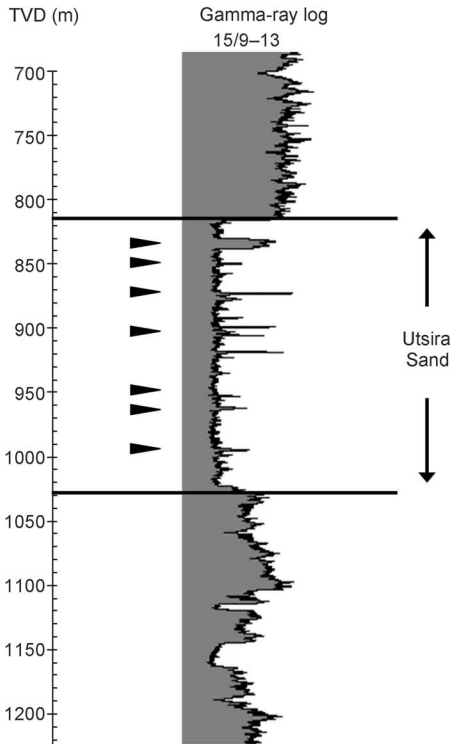

Figure 2. A well log from the Utsira Sand, showing the gamma-ray measurements. The gamma-ray values for the cap rock typically are higher than those for the sand body within Utsira. Notice the gamma-ray peaks within the Utsira Sand correspond to thin shale beds in an otherwise homogeneous thick sand layer. The thin shale layers are assumed to have typical thicknesses of 1–2 m.

Seismic time shifts usually are estimated by determining the lag that corresponds to the peak in the crosscorrelation function between the two signal traces under consideration. Another method is to pick the traveltime for the maximum amplitude peak of a well-defined seismic event. In comparing the two methods, Landrø et al. (2001) show that the simple pick method is closer to the exact time shifts than the windowed crosscorrelation, as long as the signal-to-noise ratio is larger than one-fourth. We have found that in the case of Utsira 4D seismic analysis, there is a very good correspondence between the two methods. Hence, for the subsequent analysis, we use simple picking.

The 4D amplitude analysis is the most common method of analyzing time-lapse seismic data (Landrø et al., 1999; Koster et al., 2000). Differencing and various comparison methods are used to analyze and interpret 4D seismic changes. For thin reservoir sections, the 4D amplitude signal is enhanced by tuning effects (Landrø et al., 1999). When thin CO_2 layers are injected into a relatively thick sand body, the thickness and velocity of the CO_2 layers are unknown. Therefore, we need two independent relations to determine the two unknown parameters. Here, we compare two different methods — one combining amplitude and traveltime analysis and the other combining traveltime and rock physics.

Background for injecting CO_2 in the Utsira Formation

Concerns about global warming have initiated worldwide investigation into CO_2 disposal. A promising geologic setting for storage is saline rock formations. The Sleipner field in the Norwegian North Sea, operated by StatoilHydro, is the site of a large-scale CO_2 disposal project (Eiken et al., 2000). At Sleipner, CO_2 is injected into a shallow sand formation (Utsira) 1012 m below sea level (Figure 1). The sand body is about 210 m thick around the injection point and contains some thin shale layers, seen in a well log from Utsira (Figure 2). The formation is sealed at the top by thick shale layers. Below the sand formation, several mud diapirs can be interpreted.

The CO_2 is injected at a supercritical state close to the bottom of the formation. It rises because of buoyancy effects until reaching various flow barriers such as shale layers within the sand and the top seal shale. The shale layer above the Utsira Sand is thick and extends laterally throughout the formation. It is therefore reasonable to assume that the injected CO_2 will form a plume consisting of thin CO_2 layers (lenses) below thin, heterogeneous shale layers within the thick sand body (Lindeberg et al., 2001; Arts et al., 2004). In 1999, 2.35 million tons of CO_2 were injected into the Utsira Formation; by 2001, 4.26 million tons of CO_2 had been injected. In 2002, the total injection of CO_2 was up to 4.97 million tons. A 3D seismic data set was acquired in 1994 prior to CO_2 injection, and time-lapse seismic data were acquired in 1999, 2001, 2002, 2004, and 2006.

Several studies have been published using stacked seismic data from the 1994, 1999, 2001, and 2002 surveys (Arts et al., 2004; Chadwick et al., 2004). Ghaderi and Landrø (2005) conducted a preliminary study on estimating velocity changes based on the prestack seismic data vintages from 1994 and 1999 for the Utsira Formation. In the present work, we use prestack seismic data from the base and the first three monitor surveys.

The acquisition parameters for the various surveys at Sleipner have been repeated to a high degree (Eiken et al., 2000). However, there are some changes in shotpoint interval (from 18.75 m in 1994 to 12.5 m in 1999). Because of the severe velocity reduction caused by the presence of CO_2, different velocity fields had to be used for stacking and migrating the seismic baseline and the monitor surveys. Further details regarding 4D acquisition and processing can be found in Eiken et al. (2000).

Prestack versus poststack seismic data analysis

Most 4D studies use poststack seismic data for qualitative interpretation (Landrø and Stammeijer, 2004). For quantitative 4D analysis, prestack time-lapse data have been used to estimate pressure and saturation changes simultaneously (Tura and Lumley, 1999; Landrø, 2001; Guilbot and Smith, 2002; Røste et al., 2006). For CO_2 monitoring purposes it is desirable to estimate thicknesses of the CO_2 layers as well as the velocity change caused by the CO_2 injected into the sand layer. The ultimate goal is to estimate the thickness of each CO_2 layer. However, because measured traveltime shifts depend on thickness as well as on velocity (which depends on saturation), it is crucial to estimate both parameters from the 4D seismic data. We do not know the exact CO_2 saturation, so it is hard to estimate the velocity of the sand layer containing CO_2. Therefore, prestack time-lapse seismic data might offer a way to estimate velocity and thickness changes for the CO_2 layers.

In this work, we study some of the more important time-lapse effects in the prestack domain to measure velocity and thickness changes within the reservoir. For prestack time-lapse seismic analysis, it is more practical to compare estimated velocity changes than the actual traveltime changes because the time shifts vary with offset (Røste et al., 2006).

The paper is organized as follows: In the first section, we outline some of the rock-physics properties of CO_2 and estimate velocity changes resulting from CO_2 injection using rock-physics models. These velocity estimates are compared to the changes determined from the time-lapse seismic data only. Because our technique is developed for a single-layer case, we discuss briefly how such an event was selected from the Sleipner data set. Then we derive a method combining 4D amplitude and traveltime analysis to estimate velocity and thickness changes simultaneously. This method is compared to a more conventional method combining time shifts and rock physics.

ROCK PHYSICAL PROPERTIES OF CO_2

This section investigates potential velocity changes in the Utsira Sand based on rock and fluid properties. A typical gamma-ray well log is shown in Figure 2. It clearly shows the thick Utsira Sand between 820 and 1030 m. Six or seven thin layers can be interpreted within the Utsira Sand. Apart from these layers, the sand appears to be homogeneous. The P-wave velocity is slightly above 2000 m/s within the sand layer. A 100-m-thick high-velocity shale layer overlies the Utsira Sand. Another high-velocity shale layer approximately 10 m thick is observed 20 m deeper in the sand. Apart from these high-velocity layers, the sand velocity is nearly constant.

The CO_2 bulk modulus and density variations impact velocity-change estimations and therefore are addressed. Introducing CO_2 into the Utsira Formation has a dramatic effect on reflectivity and significantly interferes with other events.

Bulk modulus of CO_2

Because of the relationship between the temperature and density of CO_2 at reservoir pressures, it is important to know the formation temperature accurately. Uncertainty in formation temperature measurements at Sleipner introduces significant uncertainty in the estimates of CO_2 bulk modulus and density, both of which are critical inputs to the Gassmann fluid substitution model. For the Utsira Formation, two measured temperatures of 27 °C (below the top of the Utsira) and 37 °C (near the injection point) are reported. At higher temperatures, the density and bulk modulus of CO_2 are lower, resulting in lower seismic velocities. However, the decrease in the seismic velocities caused by temperature variations is not very significant.

Taking the measurement uncertainties into account, we focus on calculating the bulk modulus and density of CO_2 for a range of pressure and temperature conditions considered representative of the Utsira Formation. We use CO_2Therm, a software package developed by Erik Lindeberg at SINTEF Petroleum Research, based on an equation of state derived by Span and Wagner (1996). The effects of pressure and temperature are shown in Figure 3. At the temperature interval of interest, i.e., 27°–37°C, we note a significant change in the density and bulk modulus of CO_2: For a formation undergoing a temperature increase from 27°C to 37°C (assuming a pressure of 100 bar), the bulk modulus and density of CO_2 decreases by 53% and 15%, respectively.

As CO_2 displaces brine in the Utsira Sand, there is a decrease in seismic velocity. A calibrated Gassmann model reflects this dependency of the P-wave velocity on CO_2 saturation and temperature variation (see Figure 4 and Table 1). However, the effect of temperature on the rock velocities seems less significant than from the variations in CO_2 density. As seen from Figure 4, for an increase of 10°C, the reduction in the seismic velocities is less than 6%. The variation in temperature therefore has minimal impact on seismic velocities. However, for the density changes, the temperature effect is more pronounced. For a temperature of 27°C, the density of CO_2 is close to 800 kg/m^3, which is not too different from that of water. A porosity of 37% yields a density change of 4%. Therefore, we assume in our analysis that density changes are negligible compared to velocity changes. In cases where density changes are more significant, it is straightforward to include a density change in our equations, but then this density-change estimate needs to be based on rock-physics input.

The velocity changes in the sand are tied directly to the time shifts used for volumetric estimates. Although we may be able to estimate the volume of the CO_2 layers, it might remain a challenge to estimate the total mass of the injected CO_2 because of the uncertainty in density related to actual formation temperature.

According to reservoir engineering reports for the CO_2 project at Sleipner, the expected pore-pressure changes are minor. This is caused by the excellent permeability and porosity of the Utsira Sand. Therefore, we neglect pressure effects in this study. Although some pressure variations close to the injection point will occur, we believe these effects are minor for the distal CO_2 layer we are studying.

Reflectivity of CO_2 swept sands

Previous studies (Arts et al., 2004) have shown that the 4D signal caused by the CO_2 injection into the Utsira Sand at Sleipner is strong, probably three to four times stronger than typical 4D signals from producing hydrocarbon reservoirs. As shown in Figure 5 for prestack single-offset (318 m) data, the root-mean-square (rms) amplitude increase for the entire Utsira Formation is between 1.5 and 2 when the 1994 survey is compared to the 1999 survey. Arts et al. (2004) explain this significant amplitude change by a combined effect of a significant velocity drop caused by the CO_2 and seismic tuning effects.

Using the calibrated Gassmann model presented in the previous section, we find that for the top Utsira interface, the fluid change corresponds to an increase in the reflection coefficient at zero offset by approximately four times compared to the base survey (Figure 6). This number is associated with some degree of uncertainty, mainly because the background or initial parameter values for the shale and sand vary laterally. The input parameters used to obtain the reflection

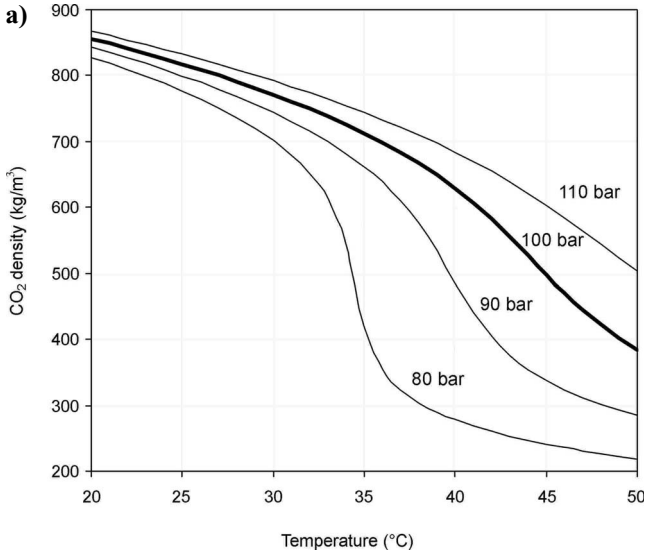

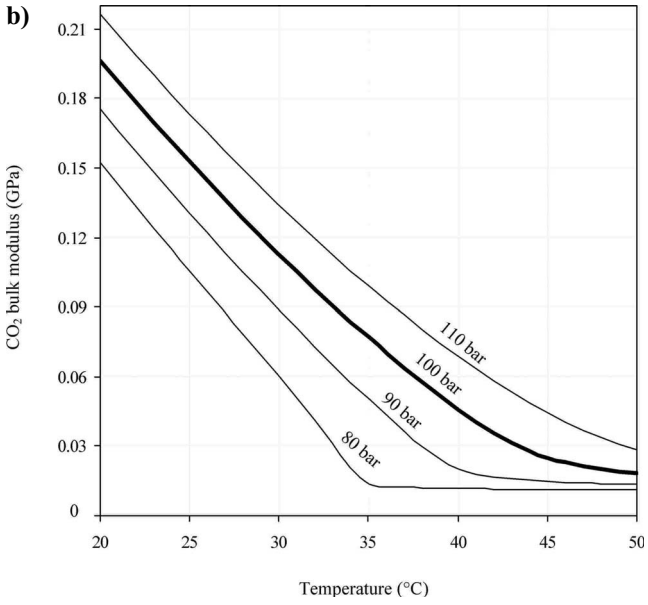

Figure 3. The (a) density and (b) bulk modulus of CO_2 as a function of temperature for four different pressure values, based on an equation of state by Span and Wagner (1996). Measurements show formation temperature between 27°C and 37°C.

Table 1. Rock properties used in the Gassmann modeling of the P-wave response to the gradual increase of CO_2. Other input parameters are $\phi = 37\%$, $K_{grain} = 36.9$ GPa, $K_{frame} = 2.56$ GPa, $V_{P_{sand}} = 2050$ m/s, $V_{S_{sand}} = 643$ m/s, and $\rho_{solid} = 2650$ kg/m^3.

Seismic parameters	K_{CO_2} (GPa)	K_{H_2O} (GPa)	ρ_{H_2O} (kg/m^3)	ρ_{CO_2} (kg/m^3)
(27°C, 100 bar)	0.136	2.28	1020	800
(37°C, 100 bar)	0.064	2.34	1070	680

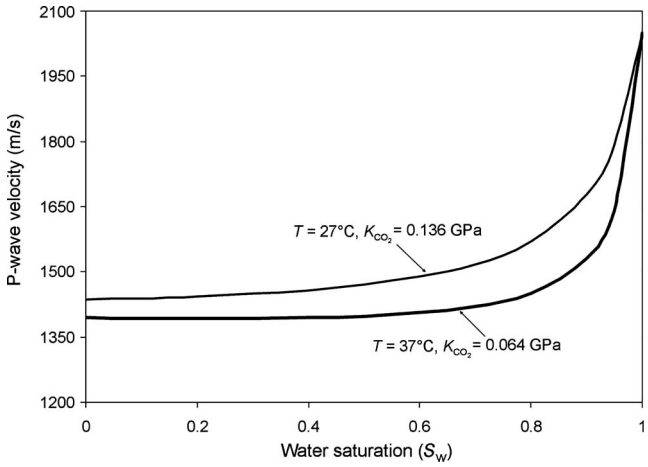

Figure 4. P-wave velocity versus changes in water saturation, based on Gassmann modeling for a fixed pressure value of 100 bar and two different values of assumed formation temperature. The CO_2 bulk modulus is K_{CO2}. The parameters used in the substitution model are given in Table 1.

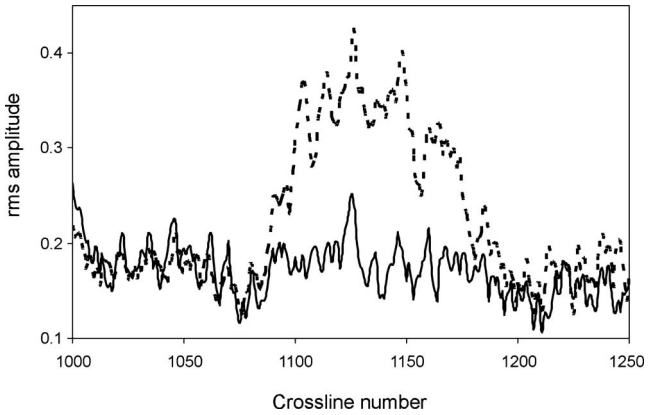

Figure 5. Seismic rms amplitude level in Utsira Formation for the single offset at 318 m and the inline 1839 passing through the CO_2 plume for a window of 400 ms. The distance between each crossline is 12.5 m. The solid line indicates the rms level in the base survey; the dotted line is rms values corresponding to the 1999 survey. An amplitude increase of about 1.9 times above the injection point and about 1.3 times for the whole inline is observed.

curves (using Smith and Gidlow's approximation from 1987) are given in Table 2. The extra amplitude increase caused by tuning effects can be up to 100% (Widess, 1973; Ostrander, 1984). A comprehensive study of the tuning effects for several of the intrasand layers is presented by Arts et al. (2004). It is also important to note that intrasand reflections (Figure 7) are not interpretable on the base survey but are stronger than the top Utsira reflection after CO_2 injection. Figure 7 shows the amplitude changes observed at top Utsira and the strongest intrareservoir event (marked M1).

The first water-layer multiple of event M1 is a strong, prominent event on the 1999 poststack data. The water depth at the injection site is about 80 m, corresponding to a multiple period of 108 ms (assuming a water velocity of 1480 m/s). For the near-offset prestack data (318 m), the amplitude ratio between the first-order multiple and event M1 is on the order of 0.6, corresponding to a sea-bottom reflection coefficient of approximately 0.3. Comparing this first-order multiple amplitude to the typical reflection strength on the base survey, we find that it is stronger or of the same strength as interpretable reflections from the base survey. This means that a conventional time-shift analysis (Landrø, 2001; Hatchell and Bourne, 2005; Røste et al., 2006) is not possible at this location without taking this multiple problem into account.

Ghaderi and Landrø (2005) attempted to avoid this issue by using reflections below the Utsira Sand that is not heavily influenced by multiples. However, these results might be inconclusive because of the interference between multiples and reflections below the reservoir. Although conventional demultiples have been applied to the poststack data, remaining multiple energy causes problems for accurate time-shift estimation. For the prestack data, no demultiple was used prior to analysis.

We therefore seek a thin CO_2 layer that does not create a strong multiple that might interfere with the base Utsira event. The multiple problems associated with such an isolated CO_2 event should be far less than for the examples we discuss.

SELECTING AN EVENT WITH MINOR MULTIPLE INTERFERENCE PROBLEMS

As described, strong multiple energy from the injected CO_2 layers situated below thin shale layers interferes with most of the reflections below the CO_2 plume. However, a single, fairly weak CO_2 response is found southwest of the injection point (see Figure 8). In Figure 9, the location of this event (marked A) is at about 960 ms and is highlighted in blue color. Because the amplitude change for the event is weaker than those in the central part of the CO_2 plume, we assume the interference between water-layer multiples from this event and other events is likely to be less pronounced. Thus, we analyze time shifts resulting from velocity changes at event A at the reflection corresponding to the base Utsira (event B).

The subsequent development of this event during the three consecutive time-lapse acquisitions is shown in Figure 10. Figure 11 shows interleaved traces from 1994 and 1999 for event B. Notice the systematic time shift for each of the pairs. This is clearly illustrated in Figure 12, where a selected trace for all four seismic surveys is compared. The reason for this systematic time

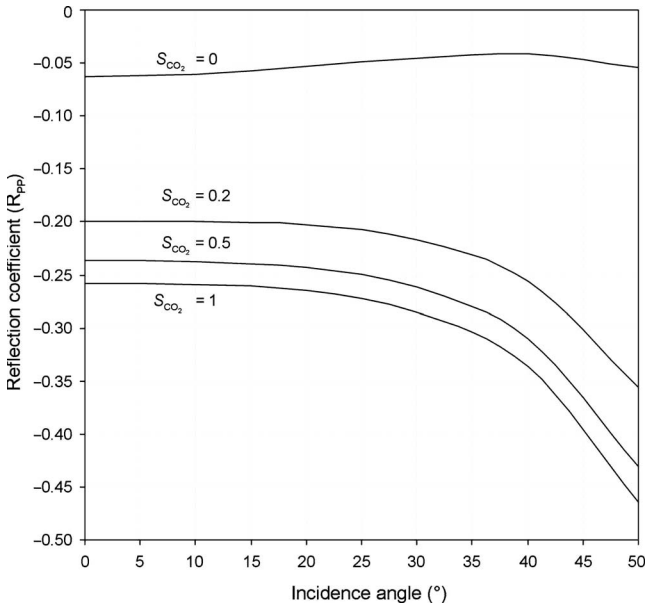

Figure 6. Modeling the Zoeppritz reflection coefficient for various incidence angles and four different CO_2 saturation values S_{CO_2}. We use a standard calibrated Gassmann type of fluid substitution.

Table 2. Seismic parameters used in the numerical example (assuming z = 820 m, p = 100 bar, and T = 27°C). Other input parameters are ϕ = 37%, $V_{P_{shale}}$ = 2270 m/s, $V_{S_{shale}}$ = 850 m/s, ρ_{shale} = 2100 (kg/m³), ρ_{solid} = 2650 kg/m³, ρ_{H_2O} = 1020 (kg/m³), and ρ_{CO_2} = 800 kg/m³.

S_{CO_2} (%)	V_P (m/s)	V_S (m/s)	ρ (kg/m³)
0	2050	643	2047
20	1568	645	2030
50	1470	649	2006
100	1437	656	1965

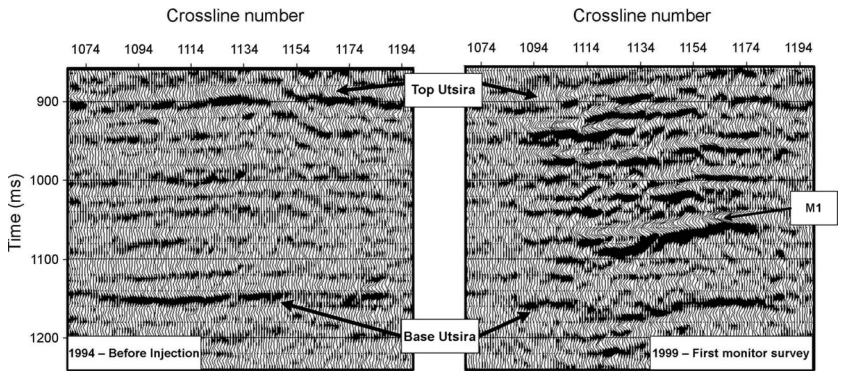

Figure 7. Two prestack seismic vintages from Utsira, illustrating effectively the presence of CO_2 through increased reflectivity caused in 1999 (right) compared to preinjection case acquisition in 1994 (left). The base Utsira reflection is shifted, and traveltime picking is obscured because of possible interference with remaining sea-bottom multiples energy from event M1 marked around 1050 ms.

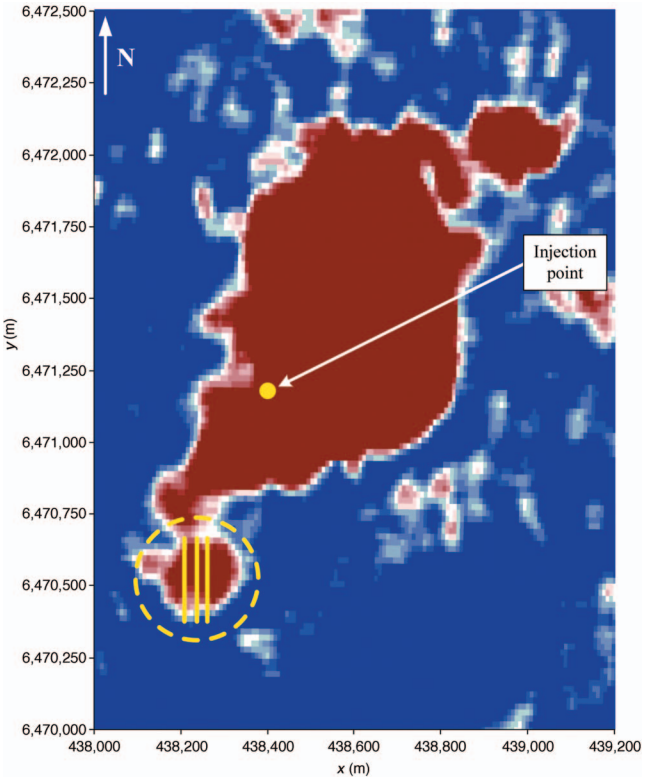

Figure 8. The rms amplitude map (using a 20-ms window centered about 970 ms) of the Utsira Sand on the 1999 survey on prestack data from the single offset at 318 m. Notice the prominent CO_2 side-plume event propagating to the southwest, marked by the dashed yellow circle. The three parallel yellow lines within the yellow circle represent the three crosslines where the amplitude and time-shift measurements have taken place.

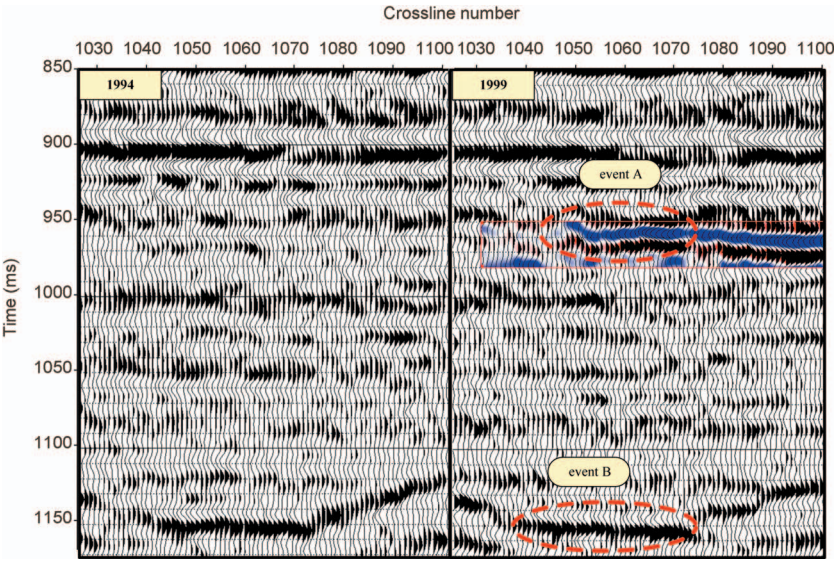

Figure 9. Side-plume event and its influence on the base of Utsira. The areas of interest are event A, which is part of the main CO_2 plume, and the part of the base of Utsira encircled by a dashed line, denoted as event B.

shift, or pushdown, is CO_2 event A, developing away from the main plume.

The amplitude pattern for event B is more complicated to explain because this is the result of the signal passing through a thin layer causing subtle interference effects that influence the amplitude level at base Utsira. The method we develop in the next section is, however, independent of amplitude measurements for the base reflector and takes into account only time shifts measured on the base reflector and the amplitude measured for event A.

THEORY — COMBINING 4D TIME SHIFT AND AMPLITUDE ANALYSIS

The attempt to estimate the velocity change caused by the presence of CO_2 in the Utsira Formation by Ghaderi and Landrø (2005) takes into account the whole plume and is based only on the time-shift measurements on the base of Utsira. This method estimates the relative change in velocity to be approximately 10%.

Traveltime shift versus offset

Consider a homogeneous medium where a thin layer is introduced (see Figure A-1, Appendix A). Assuming small offset, the relative traveltime shift caused by a single-layer event is given by (see Appendix A, equation A-9)

$$\frac{\Delta T}{T} = -\frac{\Delta V}{V}\frac{\Delta z}{z}, \tag{2}$$

where T is the two-way traveltime to the base; V and z are the velocity and thickness of the homogeneous layer, respectively; and Δz is the thickness of the CO_2 layer. For the limit $\Delta z \rightarrow z$, equation 2 reproduces equation 1. In equation 2, the relative traveltime shift is independent of offset. This implies that it is not possible to discriminate between velocity and thickness by exploiting only the relative traveltime shifts versus offset. Therefore, we introduce 4D amplitude changes as a second equation to estimate velocity and thickness changes simultaneously.

Combining 4D amplitude and traveltime information — Amplitude variation versus time shift

Consider the same simple configuration as above where a thin layer is embedded in a homogeneous layer (Figure B-1, Appendix B). Now we consider reflection from the top and base of the layer. The resulting signal from this thin layer is

$$|S_d(\omega)| = \frac{|P(\omega)|\Delta R^F}{z_1}\sin\left(\frac{\Delta z\omega}{V_2\cos\theta}\right). \tag{3}$$

Here, $P(\omega)$ is the pulse amplitude spectrum; ΔR^F is the change in reflectivity resulting from fluid saturation in the thin layer; θ is the incidence angle; V_2 and Δz are the velocity and thickness of the thin layer, respectively; and ω denotes circular frequency. Using equation 2, we see that $\Delta z/z = -(\Delta T/T)(V_1/\Delta V)$, where V_1 is the p-wave ve-

locity in sand. Substituting this into equation 3 and assuming $\Delta\rho/\rho \ll 1$ results in

$$|S_d(\omega)| = \frac{|P(\omega)|\omega}{2V_1\cos^3\theta}\frac{\Delta T}{T} \times \mathrm{sinc}\left(-\frac{\Delta T}{T}\frac{z_1\omega}{\Delta V\cos\theta}\right). \quad (4)$$

A well calibration to the top Utsira can be used to determine the amplitude value of the effective pulse P in equation 4. Note that P includes transmission and absorption losses and is not the same as the source wavelet measured in, for instance, the water layer. However, if one assumes that a proper well tie can be done to an interface close to the CO_2 layer, it is possible to determine P.

This is an interesting result because the only unknown in equation 4 is ΔV. Combining equation 4 with equation 2, we can determine the thickness Δz. This means that it is possible to estimate the CO_2 thickness, given that the reflection coefficient of the top of the CO_2 anomaly can be estimated from the seismic amplitude and that the traveltime shift caused by this anomaly is measured on an interface below the anomaly.

FIELD DATA EXAMPLE

Here, we test the methodology using prestack seismic data from the selected areas of the seismic vintages shown in Figure 10. In addition, we also test the direct method using time shifts and rock physics. In Figure 10, a somewhat weaker seismic event (around 1070 ms) occurs below target event A (which is around 960 ms in Figure 9) in surveys from 2001 and 2002. The traveltime difference between these two events and the amplitude ratio indicate this is a multiple. However, we cannot rule out the possibility that this event is a second CO_2 layer. Despite this, we assume that the influence of this event is negligible for our analysis, mainly based on the much weaker amplitude for this event.

Estimating the source amplitude

To estimate the pulse amplitude of the seismic source wavelet P, we use the top of the Utsira Formation for calibration. From well logs, we estimate a zero-offset reflection coefficient of -0.063. The average measured seismic amplitude for this event is $S_d = 0.36$. The depth of top Utsira is approximately 820 m and average two-way traveltime is 890 ms, yielding an approximate estimate for the pulse strength (using equation B-1) of

$$P = \frac{2zS_d}{T^2R_0} \approx \frac{2\times 820\times 0.46}{(0.89)^2\,0.063} = 11{,}943. \quad (5)$$

It is important to note that this simple procedure involves significant uncertainties in the pulse estimate because there are large uncertainties involved in the estimate for the zero-offset reflection coefficient as well as the average amplitude strength measured at top Utsira. Despite these uncertainties, we use this value for all surveys. This means that by choosing a constant value for P, the relative changes in our estimated thickness and velocity changes should suffer less from this uncertainty, but there could still be an absolute error that is unaccounted for. Picking near-offset amplitudes over a large

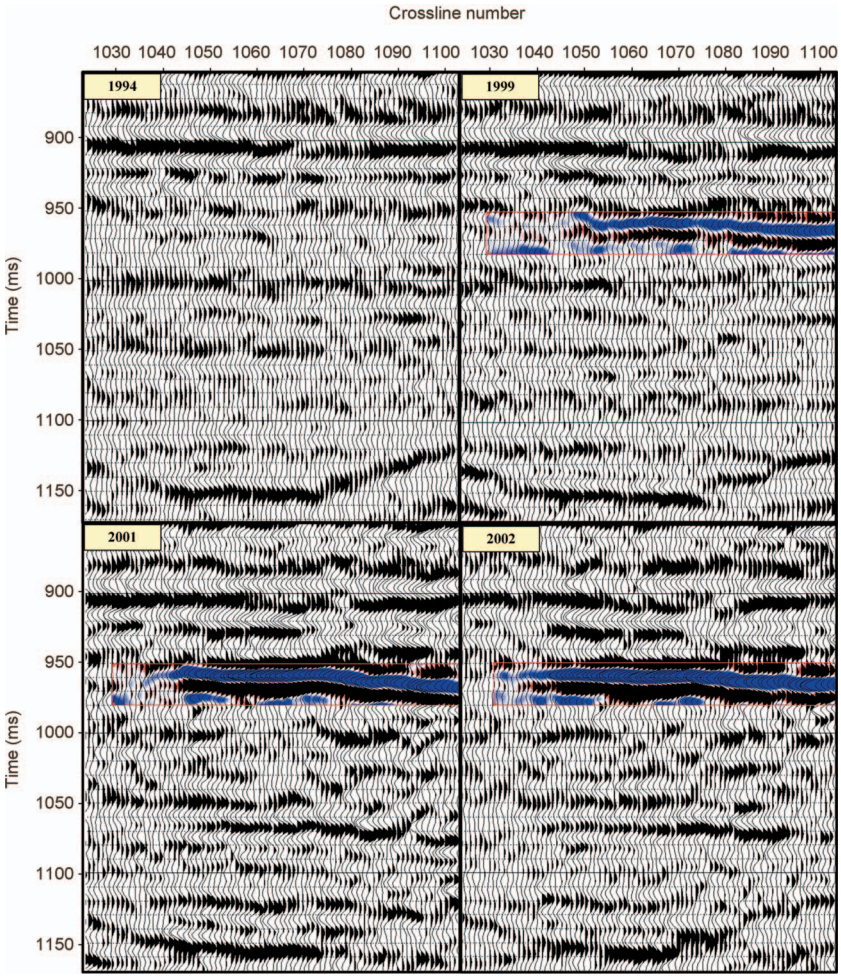

Figure 10. Side-plume event during the three time-lapse 3D seismic surveys. The distance between each crossline is 12.5 m.

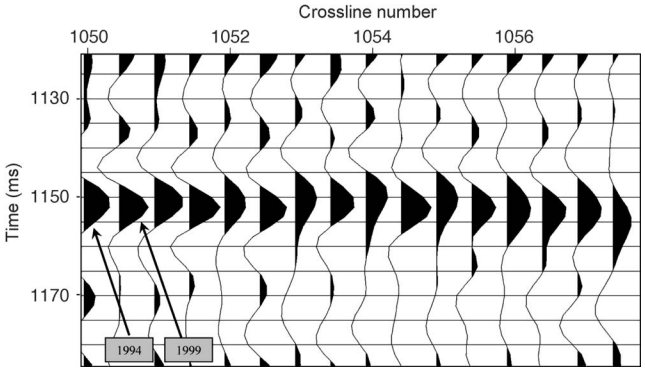

Figure 11. Constant-offset (318 m) traces at event B, with interleaved traces from 1994 (left) and 1999 (right). Notice the systematic shift for each pair of traces.

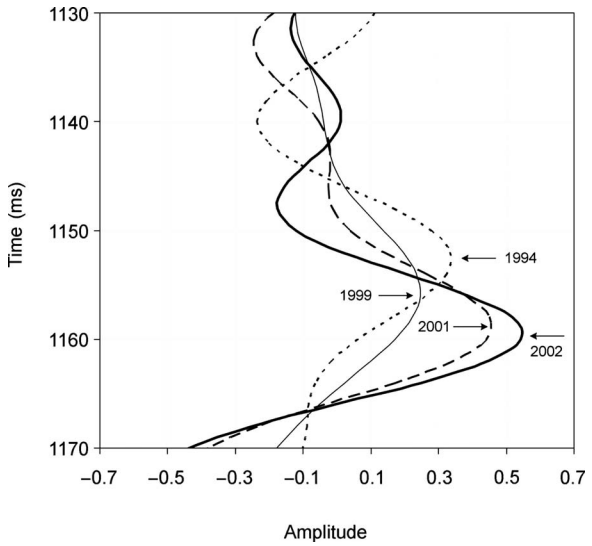

Figure 12. Effect of the CO_2 plume on the base of the Utsira Sand on a selected trace, corresponding to (inline, crossline) = (1821, 1060) at event B. Note the systematic increase in the time shifts after each survey. Also, the amplitude effects are quite prominent.

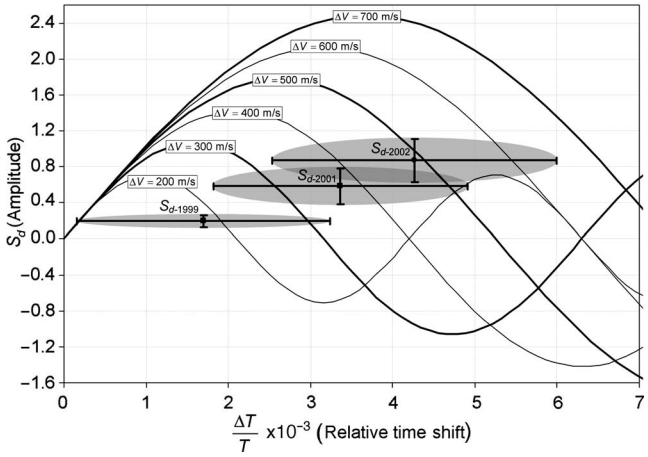

Figure 13. Amplitude variation versus the relative traveltime shift. The single points correspond to the actual measured amplitude data from each of the time-lapse vintages in 1999, 2001, and 2002. Each point corresponds to an average of measurement values from three crosslines, where the bars indicate the standard deviation and the shaded area indicates the spread of data. The curves correspond to the theoretical model based on equation 4. Each curve is labeled with the value of the velocity change.

Table 3. Variation in the thickness of the CO_2 layer according to the method of combining time shifts and 4D amplitudes.

Survey year	ΔV (m/s)	Δz (m)
1999	200	15
2001	400	15
2002	500	15

area (4000 common depth points) gave a standard deviation for S_d of 0.029 or 8%. The uncertainty in the reflection coefficient is probably larger because variation in cap-rock properties and inaccuracies introduced by upscaling from well logs introduce systematic errors in the estimated reflection coefficient.

Estimation of velocity and thickness changes using 4D time shifts and amplitude changes

From equation 4, we observe that there might be several values of the unknown ΔV parameter giving the same observed S_d value. For simplicity, we introduce a simple graphical solution procedure as shown in Figure 13. The measured 4D seismic data are shown with their estimated standard deviations (one standard deviation) for both of the measured parameters (relative time shifts along the horizontal axis and 4D amplitude changes along the vertical axis). The combined effect of the two standard deviations gives rise to the shaded ellipses in the figure, and our strategy is to choose solutions from the modeled curves that are as close as possible to the center of the three ellipses.

For the modeled curves in Figure 13, the following parameters were used: $f = 50$ Hz, $\theta = 9.6°$, $V_1 = 1850$ m/s, and $z_1 = 943$ m. For the overburden velocity V_1, an average value has been used, and the depth of the overburden is taken from the well log.

From an estimate of the velocity change ΔV, the variation in thickness is calculated as (equation 2)

$$\Delta z = -z_1 \frac{V_1}{\Delta V} \frac{\Delta T}{T}. \tag{6}$$

The results are given in Table 3.

Estimation of velocity and thickness changes using traveltime shifts and rock physics

If we assume that the average velocity within the CO_2 layer and the corresponding relative velocity change (caused by the CO_2 injection) are known from rock-physics measurements or a calibrated Gassmann model, we can exploit this information to estimate the thickness of a thin CO_2 layer within a homogeneous background model.

In this case, we assume that the CO_2 is trapped below a thin shale layer and that the shale layer is thin compared to the thickness of the CO_2 layer. Typically, we assume that the shale layer is only 1–2 m thick and that the CO_2 layer is around 10–20 m. If the relative velocity change is known, we can use equation 2 directly to estimate the thickness change. A slightly more accurate method for the zero-offset case can be derived as follows:

$$\Delta T_0 = \frac{2\Delta z}{V_2} - \frac{2\Delta z}{V_1}, \tag{7}$$

where V_1 and V_2 are the velocities before and after CO_2 injection, respectively, and Δz is the thickness of the CO_2 layer. If we assume that

ΔT_0 can be measured at an interface below the CO_2 layer, the thickness of the CO_2 layer is

$$\Delta z = \frac{V_1 V_2}{2(V_1 - V_2)} \Delta T_0. \quad (8)$$

As discussed previously, for the Utsira Formation at Sleipner, typical values for velocities from well-log analysis for 100% water-saturated sand at 2050 m/s and assuming that the end state is fully CO_2 saturated, we obtain a velocity of 1440 m/s. Using these values in equation 8 yields

$$\Delta z \approx 2400 \Delta T_0, \quad (9)$$

assuming that the time shift is estimated in seconds. In practice, however, we do not know the CO_2 saturation; hence, the velocity change between monitor and base surveys might be associated with significant uncertainties. Figure 14 shows estimated zero-offset (we assume 318 m is close to zero offset) traveltime shifts for a selected inline at Utsira. Using equation 9, we estimate the CO_2 thicknesses. The results are given in Table 4.

The major difference between the two methods is that the method combining amplitude and traveltime shifts gives a gradual decrease in velocity over calendar time; the rock-physics-based method predicts constant velocity change. Hence, the first method predicts a more-or-less constant thickness of the CO_2 layer, whereas the second method predicts a constant velocity and a gradual increase in the thickness of the CO_2 layer.

A possible explanation for the lower velocity-change value in 1999 compared to the Gassmann prediction is that the saturation distribution is more patchy in 1999 than in 2001 and 2002. By patchy distribution, we mean there might be one or two thin shale layers within the thickness of 15 m that trap individual CO_2 layers with a thickness below seismic resolution. Changes in amplitudes because of saturation differences within Utsira are addressed by Carcione et al. (2006). They relate varying saturation to the presence of thin, isolated shale layers. They find that the P-wave velocity discriminates between uniform and patchy saturations for brine saturations above 60%. They support their conclusion by numerical modeling, taking into account patchy saturation and attenuation.

DISCUSSION

A major objective of this work is to develop a quantitative 4D analysis method to estimate CO_2 velocity and layer-thickness changes. These estimates can be used to estimate the volume of injected CO_2 into a saline aquifer. To illustrate this, we have used time-lapse seismic data from 1999, 2001, and 2002 acquired at the Sleipner field. To simplify the analysis, we selected a case where the CO_2-saturated layer is isolated from the main plume. The results obtained for the CO_2 thickness are 15 m for all three vintages, leading to expectation that the velocity is also constant. However, the estimated velocity changes are 200, 400, and 500 m/s for the three vintages. One possible way to interpret this result is to introduce patchy saturation changes within the 15-m-thick CO_2 layer. On the other hand, fixing the velocity change to 30% reduction leads to a gradual increase in the CO_2 layer thickness.

It is not straightforward to implement our method of combining time-shift and amplitude analysis for multiple layers of CO_2 because the time shift measured for an interface below the sand layer will provide information only about the average time shift for all CO_2 layers stacked above each other. A way to circumvent this problem might be to use a single-layer plume, as described here, to determine the velocity change and then to assume that the velocity change is more or less constant for the multistack case. However, this assumption means that the CO_2 saturation for all layers must be approximately equal, and that is unlikely.

Therefore, other methods must be developed to handle this case. One approach might be to consider amplitude changes versus offset, similar to a procedure used by Landrø (2001) to separate pressure and saturation changes in the time-lapse data. But because we have to assume thin layers, the amplitude changes with offset might be harder to resolve for independent estimates of velocity and thickness changes. Another approach to solve the multilayer CO_2 problem is to combine reservoir fluid-flow simulation with seismic 4D modeling and invert for velocity and thickness changes. However, such an approach requires knowledge of vertical and horizontal permeability distributions within the heterogeneous sand layer.

Because the equation derived for estimating the velocity change from time-shift and amplitude changes has multiple solutions (inverse of a sinc function), we propose a graphical technique to visualize various solutions and compare to the observed 4D data. The spread in the estimated time shifts is significant, and this leads to significant uncertainties in the estimated velocity and thickness changes.

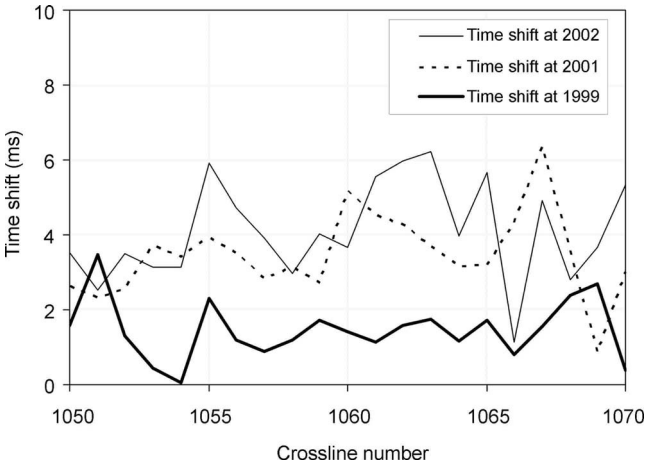

Figure 14. Estimated time shift caused by the CO_2 side-plume event, measured on the base of the Utsira Sand.

Table 4. Thickness variation of the CO_2 layer according to rock physics and time shifts from seismic data and equation 9.

Thickness variation (m)	1999	2001	2002
Δz	4	8	10

CONCLUSIONS

Injection of CO_2 into a sand layer causes significant amplitude and traveltime changes on time-lapse seismic data. Based on field data from the Sleipner CO_2 storage project, we find that it is possible to discriminate between velocity and thickness changes caused by CO_2 injection. Thin CO_2 layers are formed below even thinner shale layers within the sand body where the CO_2 is injected.

All analysis is done on a near-offset narrow stack (offset range 243-393 m). We estimate a velocity change of around 200 m/s three years after injection start and 500 m/s two to three years later.

A combination of 4D amplitude and time-shift analysis enables us to discriminate between velocity and thickness changes within thin CO_2 layers. The 4D amplitude analysis is based on simple tuning equations. Our method is limited to only one CO_2 layer within the sand body, and the method is tested successfully for such a single-layer event. Most of the CO_2 layers caused by the injection, however, are stacked on top of each other as separated layers (typically 20–50 m between each layer).

When 4D time shifts and 4D amplitude changes are combined to estimate velocity and thickness changes simultaneously, we find that the thickness for a single CO_2 layer at Utsira remains constant from 1999 to 2002 (15 m); the velocity gradually changes from 200 m/s in 1999 to 400 m/s in 2001 and 500 m/s in 2002. If we fix the velocity change by using rock physics (Gassmann) and assume a constant CO_2 saturation for the entire layer, we find that the thickness of the CO_2 layer increases from 4 m in 1999 to 8 m in 2001 and to 10 m in 2002. These results are not too far from each other because a lower velocity change will mean several thin, separated CO_2 layers in a patchy saturation case, leading to an effective thickness less than 15 m.

ACKNOWLEDGMENTS

StatoilHydro and the CO_2STORE project partners are acknowledged for permission to use and present the geophysical data. We would also like to thank Ola Eiken, StatoilHydro, for support and discussions. Erik Lindeberg, SINTEF, is acknowledged for numerous technical discussions and for providing his CO_2Therm tool to calculate the thermodynamic properties of CO_2. The Research Council of Norway is acknowledged for financing the work through the KMB project "EOR by CO_2 Injection and Deposition in Aquifers" at SINTEF Petroleum Research. Also thanks are given to the ROSE (Rock-Seismic) project sponsored by the Norwegian Research Council (NFR) and IO-Center (Integrated Operations) at NTNU for financing part of this work. Eirik Fossgaard is acknowledged for careful review and finding an error in one of the equations and Alexey Stovas for the correction to the equation. Finally, we thank the reviewers, three anonymous and David Johnston, for numerous suggestions that improved this paper significantly.

APPENDIX A

TIME SHIFT VERSUS OFFSET

When CO_2 is injected into an aquifer formation, new thin CO_2 layers might appear below thin shale layers (typically 1–3 m thick). Because of the strong velocity decrease caused by the CO_2 injection, these layers are observed as strong events.

Figure A-1 shows a case where one such CO_2 layer is created within a homogeneous sand layer. Consider the sketch on the left in Figure A-1. This represents a homogeneous aquifer sand body. The sketch on the right represents the situation when a thin layer of CO_2 is introduced. From the figure, we note that $z = z_1 + \Delta z + z_2$, θ is the angle in the nonperturbed media prior to CO_2 injection, and θ_1 and θ_2 are incidence angles for the perturbed media caused by CO_2, shown in Figure A-1.

The two-way traveltimes in the unperturbed and perturbed media are given as

$$T_1 = \frac{2z}{V\cos\theta}, \tag{A-1}$$

$$T_2 = \frac{2z}{V\cos\theta}\left[\left(1 - \frac{\Delta z}{z}\right)\frac{\cos\theta}{\cos\theta_1} + \frac{\Delta z}{z\left(1 + \dfrac{\Delta V}{V}\right)}\frac{\cos\theta}{\cos\theta_2}\right]. \tag{A-2}$$

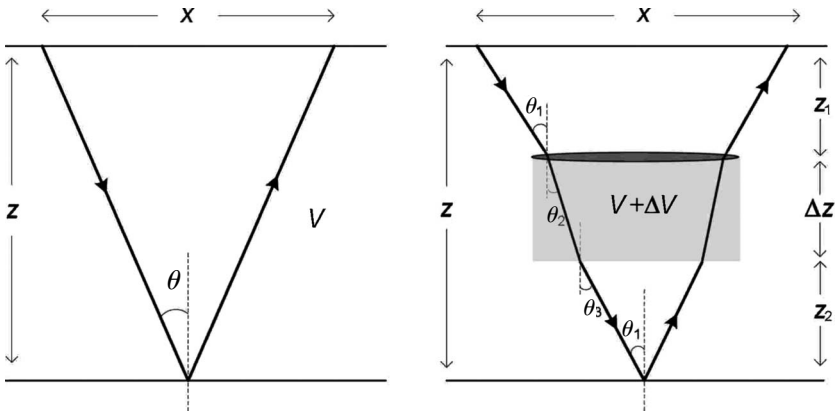

Figure A-1. Base (left) and monitor (right) cases, representing pre- and post-CO_2 injection. The objects are not to scale and are exaggerated for clarity. It is assumed that the shale layer is much thinner than the CO_2 layer and its effect on traveltime is not taken into account in calculations but is included in the figure above the CO_2 layer for illustration.

The relative time shift is then given as

$$\frac{\Delta T}{T_1} = \left(1 - \frac{\Delta z}{z}\right)\sqrt{\frac{1 + \tan^2\theta_1}{1 + \tan^2\theta}} + \frac{\dfrac{\Delta z}{z}}{\left(1 + \dfrac{\Delta V}{V}\right)}\sqrt{\frac{1 + \tan^2\theta_2}{1 + \tan^2\theta}} - 1. \tag{A-3}$$

The fixed-offset condition means that ($x_1 = x_2$)

$$\tan\theta = \left(1 - \frac{\Delta z}{z}\right)\tan\theta_1 + \frac{\Delta z}{z}\tan\theta_2. \tag{A-4}$$

We also recall Snell's law:

$$\sin\theta_2 = \left(1 + \frac{\Delta V}{V}\right)\sin\theta_1. \quad \text{(A-5)}$$

By combining equations A-4 and A-5, it is possible to show that

$$\tan\theta_2 \approx \tan\theta_1\left(1 + \frac{\Delta V}{V\cos^2\theta_1}\right) \quad \text{(A-6)}$$

and

$$\tan\theta \approx \tan\theta_1\left(1 + \frac{\Delta V\Delta z}{Vz\cos^2\theta_1}\right). \quad \text{(A-7)}$$

Inserting equations A-6 and A-7 into equation A-3 and using the Taylor expansion to the third order yields

$$\frac{\Delta T}{T} = -\frac{\Delta V}{V}\frac{\Delta z}{z}\left[1 + \frac{\Delta V}{V}\left(\tan^2\theta - 1 - \frac{1}{2}\tan^4\theta - \frac{1}{2}\frac{\tan^2\theta}{\cos^2\theta}\right)\right]. \quad \text{(A-8)}$$

A simpler approximation that can be derived from equations A-6 and A-7 is

$$\frac{\Delta T}{T} = -\frac{\Delta V}{V}\frac{\Delta z}{z}\left(1 - \frac{\Delta V}{V}\cos^2\theta\right). \quad \text{(A-9)}$$

For larger values of $\Delta V/V$, it is recommended to keep the term in the denominator, that is,

$$\frac{\Delta T}{T} = -\frac{\Delta V}{V}\frac{\Delta z}{z\left(1 + \frac{\Delta V}{V}\cos^2\theta\right)}. \quad \text{(A-10)}$$

APPENDIX B

AMPLITUDE RESPONSE OF A THIN CO_2 LAYER

Consider a CO_2 layer of thickness Δz, embedded in a homogeneous layer with a background velocity V_1. Furthermore, assume that the depth of the CO_2 layer is z_1 and the velocity of the layer is V_2 (see Figure B-1). For such a model, if the reflection coefficient of the top of the CO_2 layer is R_0, then the reflection coefficient for the bottom of the thin layer is $-R_0$. Hence, the signals reflected from the top and the base of the thin CO_2 layer are given as

$$S_1(t) = \frac{1}{2z_1}P\left(t - \frac{2z_1}{V_1}\right)R_0,$$
$$S_2(t) = \frac{1}{2(z_1 + \Delta z)}P\left(t - \frac{2z_1}{V_1} - \frac{2\Delta z}{V_2}\right)(-R_0). \quad \text{(B-1)}$$

Here, $P(t)$ denotes the seismic source wavelet. Assuming that $\Delta z \ll z_1$, the amplitude spectrum of the resultant signal reflected from this layer is given as

$$|S_d(\omega)| = \left(\frac{R_0}{z_1}\right)|P(\omega)|\sin\left(\frac{\Delta z\omega}{V_2}\right). \quad \text{(B-2)}$$

The traveltime change caused by the presence of CO_2 (assuming zero offset and that $t_1 = 2z_1/V_1 + 2\Delta z/V_1$ and $t_2 = 2z_1/V_1 + 2\Delta z/V_2$) is

$$\Delta t = -\frac{2\Delta z}{V_2}\frac{\Delta V}{V_1}. \quad \text{(B-3)}$$

Now, still assuming a zero-offset reflection $\rho_0 \approx \rho_1$, $\Delta V \ll V_1$, and using equation B-3, the reflection coefficient at zero offset can be approximated by

$$R_0 \approx -\Delta t\frac{V_2}{4\Delta z}. \quad \text{(B-4)}$$

Substituting equation B-4 into equation B-2 and solving for Δz, we obtain an explicit expression for the thin-layer thickness, given as

$$\Delta z = \frac{V_2}{\omega}\text{sinc}^{-1}\left(-\frac{4S_d(\omega)z_1}{\Delta t\omega P(\omega)}\right), \quad \text{(B-5)}$$

where sinc^{-1} is inverse of the sinc function, $\text{sinc}(x) = \sin x/x$.

So far, we have been looking into vertical incident signals to the thin bed. For nonzero incident angles θ, the thickness Δz of the CO_2 layer is expressed as $\Delta z/\cos\theta$. This results in generalization of equation B-2 to

$$|S_d(\omega)| = \left(\frac{R_0}{z_1}\right)|P(\omega)|\sin\left(\frac{\Delta z\omega}{V_2\cos\theta}\right). \quad \text{(B-6)}$$

The change in reflectivity caused by fluid saturation change in the thin layer for nonzero incidence angle is (Landrø, 2001)

$$\Delta R^F \approx \frac{1}{2}\left(\frac{\Delta\rho}{\rho} + \frac{\Delta V}{V_1}\right) + \frac{\Delta V}{2V_1}\tan^2\theta. \quad \text{(B-7)}$$

Inserting equation B-7 into B-6 results in

$$|S_d(\omega)| = \frac{|P(\omega)|}{2z_1}\left(\left[\frac{\Delta\rho}{\rho} + \frac{\Delta V}{V_1}\right] + \frac{\Delta V}{V_1}\tan^2\theta\right)\sin\left(\frac{\Delta z\omega}{V_2\cos\theta}\right). \quad \text{(B-8)}$$

From equation 2, we see that $\Delta z/z = -(\Delta T/T)(V_1/\Delta V)$. Accordingly, the sinus argument in equation B-8 could be expressed as $-(\Delta T/T)(z_1\omega/\Delta V\cos\theta)$. Substitution in equation B-8, rearranging and assuming that $\Delta\rho/\rho \ll 1$, gives

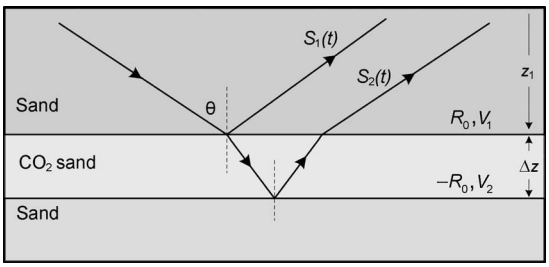

Figure B-1. Schematics of reflection from a thin layer.

$$|S_d(\omega)| = \frac{|P(\omega)|\omega}{2V_1 \cos^3\theta}\frac{\Delta T}{T}\,\mathrm{sinc}\left(-\frac{\Delta T}{T}\frac{z_1\omega}{\Delta V \cos\theta}\right). \tag{B-9}$$

Solving for ΔV gives

$$\Delta V = -\frac{z_1\omega\dfrac{\Delta T}{T}}{\cos\theta \times \mathrm{sinc}^{-1}\left[\dfrac{2S_d(\omega)V_1\cos^3\theta}{\omega P(\omega)}\left(\dfrac{\Delta T}{T}\right)^{-1}\right]}. \tag{B-10}$$

The result in equation B-10 combined with equation 2 determines the tuning thickness Δz.

REFERENCES

Arts, R., O. Eiken, R. A. Chadwick, P. Zweigel, L. van der Meer, and B. Zinszner, 2004, Monitoring of CO_2 injected at Sleipner using time-lapse seismic data: Energy, **29**, 1383–1392.

Carcione, J. M., S. Picotti, D. Gei, and G. Rossi, 2006, Physics and seismic modeling for monitoring CO_2 storage: Pure and Applied Geophysics, **163**, 175–207.

Chadwick, R. A., R. Arts, O. Eiken, G. A. Kirby, E. Lindeberg, and P. Zweigel, 2004, 4D seismic imaging of an injected CO_2 plume at the Sleipner field, central North Sea, *in* R. Davies, J. Cartwright, S. Stewart, M. Lappin, and J. Underhill, eds., 3D seismic data: Application to the exploration of sedimentary basins: Geological Society of London Memoirs, 29, 305–314.

Eiken, O., I. Brevik, R. Arts, E. Lindeberg, and K. Fagervik, 2000, Seismic monitoring of CO_2 injected into a marine aquifer: 70th Annual International Meeting, SEG, Expanded Abstracts, 1623–1624.

Ghaderi, A., and M. Landrø, 2005, Pre-stack estimation of time-lapse seismic velocity changes — An example from Sleipner CO_2-sequestration project, *in* E. S. Rubin, D. W. Keith, and C. F. Gilboy, eds., Greenhouse gas control technologies: Elsevier Science Publ. Co., Inc., 633–641.

Guilbot, J., and B. Smith, 2002, 4-D constrained depth conversion for reservoir compaction estimation: Application to Ekofisk field: The Leading Edge, **21**, 302–308.

Hatchell, P. J., and S. J. Bourne, 2005, Measuring reservoir compaction using time-lapse time shifts: 75th Annual International Meeting, SEG, Expanded Abstracts, 2500–2503.

Koster, K., P. Gabriels, M. Hartung, J. Verbeek, G. Deinum, and R. Staples, 2000, Time-lapse seismic surveys in the North Sea and their business impact: The Leading Edge, **19**, 286–293.

Kvam, Ø., and M. Landrø, 2005, Pore pressure detection sensitivities tested with time-lapse seismic data: Geophysics, **70**, no. 6, O39–O50.

Landrø, M., 2001, Discrimination between pressure and fluid saturation changes from time-lapse seismic data: Geophysics, **66**, 836–844.

Landrø, M., P. Digranes, and L. K. Strønen, 2001, Mapping reservoir pressure and saturation changes using seismic methods — Possibilities and limitations: First Break, **19**, 671–677.

Landrø, M., and R. Janssen, 2002, Estimating compaction and velocity changes from time-lapse near and far offset stacks: 64th Conference and Exhibition, EAGE, Extended Abstracts, P036.

Landrø, M., O. A. Solheim, H. Eilert, B. O. Ekren, and L. K. Strønen, 1999, The Gullfaks 4D seismic study: Petroleum Geoscience, **5**, 213–226.

Landrø, M., and J. Stammeijer, 2004, Quantitative estimation of compaction and velocity changes using 4D impedance and traveltime changes: Geophysics, **69**, 949–957.

Lindeberg, E., P. Zweigel, P. Bergmo, A. Ghaderi, and A. Lothe, 2001, Prediction of CO_2 pattern improved by geology and reservoir simulation and verified by time-lapse seismic: Proceedings of the 5th International Conference on Greenhouse Gas Control Technologies, 372–377.

Ostrander, W. J., 1984, Plane-wave reflection coefficients for gas sands at nonnormal angles of incidence: Geophysics, **49**, 1637.

Røste, T., A. Stovas, and M. Landrø, 2006, Estimation of layer thickness and velocity changes using 4D prestack seismic data: Geophysics, **71**, no. 6, S219–S234.

Smith, G. C., and P. M. Gidlow, 1987, Weighted stacking for rock property estimations and detection of gas: Geophysical Prospecting, **25**, 993–1014.

Span, R., and W. Wagner, 1996, A new equation of state for carbon dioxide covering the fluid region from the triple-point temperature to 1100 K at pressures up to 800 MPa: Journal of Physical and Chemical Reference Data, **25**, 1509–1596.

Tura, A., and D. Lumley, 1999, Estimating pressure and saturation changes from time-lapse AVO data: 69th Annual International Meeting, SEG, Expanded Abstracts, 1655–1658.

Widess, M. B., 1973, How thin is a thin bed?: Geophysics, **38**, 1176–1180.